Distinguishing Molecular Mechanical Action from Photothermal and Photodynamic Behavior

Jacob L. Beckham,[#] Thomas S. Bradford,[#] Ciceron Ayala-Orozco, Ana L. Santos, Dallin Arnold, Alexis R. van Venrooy, Víctor García-López, Robert Pal, and James M. Tour**

J. L. Beckham, C. Ayala-Orozco, D. Arnold, A. R. van Venrooy.
Department of Chemistry, Rice University, 6100 Main Street MS 222, Houston, TX 77005 USA.

T. S. Bradford, R. Pal.
Department of Chemistry, Durham University, South Road, Durham, DH1 3LE, UK

A. L. Santos.
Department of Chemistry, Rice University, 6100 Main Street, MS, 222, Houston, TX 77005 USA.
IdISBA - Fundación de Investigación Sanitaria de las Islas Baleares, Palma, Spain

V. Garcia-Lopez.
Department of Chemistry, Louisiana State University, Baton Rouge, Louisiana 70803.

Prof. J. M. Tour
Department of Chemistry, Smalley-Curl Institute, NanoCarbon Center, Rice Advanced Materials Institute, Department of Materials Science and Nanoengineering, Department of Computer Science, Rice University, 6100 Main Street MS 222, Houston, TX 77005 USA.

*Email: robert.pal@durham.ac.uk, tour@rice.edu

Keywords: molecular machines; biological materials; photomechanical, photodynamic therapy, reactive oxygen species

Abstract Text. Molecular motors (MM) are molecular machines, or nanomachines, that rotate unidirectionally upon photostimulation and perform mechanical work on their environment. In the last several years, we have shown that the photomechanical action of MM can be used to permeabilize lipid bilayers, thereby killing cancer cells and pathogenic microorganisms and controlling cell signaling. Our work contributes to a growing acknowledgement that the molecular actuation characteristic of these systems is useful for various applications in biology. However, the mechanical effects of molecular motion on biological materials are difficult to disentangle from photodynamic and photothermal action, which are also present when a light-absorbing fluorophore is irradiated with light. Here, we offer an overview of the key methods we and other research groups use to distinguish the effects of photomechanical, photodynamic, and photothermal action. We anticipate that this discussion will be helpful to the community seeking to use MM to develop new and distinctive medical technologies that result from mechanical disruption of biological materials.

1. Introduction

Molecular motors (MM) are molecular nanomachines that rotate unidirectionally and exert mechanical forces on their environment when activated by a stimulus, typically light.[1–3] Over the last 20 years, the synthesis, rotary properties, and excited-state dynamics of MM based on sterically overcrowded alkenes, also referred to as Feringa motors, have advanced to the point where motors rotating in the MHz-speed regime[4,5] are now able to perform tasks such as to locomote on a surface[6] or in solution.[7] In the last several years, MM have been shown to have a wide range of photomechanical applications in the medical field, including the mechanical opening of lipid bilayers,[8] inducing cancer cells to necrose,[9] killing microorganisms,[10–12] facilitating ion transport in cells,[13,14] and controlling mechanosensitive cell signaling pathways.[15,16]

The appeal of MM in medicine centers on the principle that the biological effects they elicit depend in some way on the ability of MM to actuate in response to irradiation. In some cases, these effects are thought to be directly driven by MM exerting mechanical force on tissue.[8,17] In other cases, the effects are attributed to some other downstream effect, such as local increases in temperature, caused by the molecular motion of the MM.[18,19] However, isolating the effects of molecular actuation is challenging. The irradiation of light-absorbing molecules within cells is known to drive a wide variety of effects outside of molecular motion, especially photothermal[20] and photodynamic[21] effects. In photothermal systems, heat generation is used to drive a desired biological outcome. In photodynamic systems, the generation of reactive oxygen species (ROS), including superoxide, hydroxyl radicals, or other reactive radicals, is used for the same. Both strategies have shown promise as approaches for disease diagnosis and treatment.[20-21] However, to develop therapeutics leveraging the unique behavior of MM, we must be able to distinguish between the effects of molecular actuation and the potential photothermal and photodynamic confounding effects also present in photostimulation experiments.[22]

To distinguish the effects of the various phenomena caused by the irradiation of light-absorbing fluorophores and to isolate the effects of molecular motion, researchers have adopted a diverse set of criteria and methods. Here, we offer a perspective from our group that uses a mixture of new experiments and previous work to detail the methodology we use to distinguish photomechanical, photodynamic, or photothermal effects driven by the activation of different types of MM with light. We also include select work from other groups, highlighting particularly useful experiments and surprising results that further develop the discussion. In the process, we aim to provide an experimental roadmap for the investigation of the underlying mechanisms driving various light-driven effects in biology. We hope that this discussion will contribute to a robust criterion for identifying the influence of molecular motion on biological and medical outcomes.

2. Investigating the Effects of Photomechanical Action.

A negative control molecule with known rotary properties serves as the linchpin to isolate the effects of molecular motion. An ideal negative control system should mimic the properties of the experimental system as closely as possible while changing its photomechanical properties in a known way. In our work, we use slow-rotating and non-unidirectional controls alongside fast, unidirectional MM to serve as these negative controls.[8] These slow or non-unidirectional MM are typically designed to be as chemically similar to our fast, unidirectional lead compounds as possible while following motor designs with previously studied rotary properties. Slow-rotating MM are designed through the use of rotor and stator structures that invoke steric hindrance during the thermal helix inversion, the rate-limiting step in motor actuation (see Figure S1 for a depiction of motor actuation).[4,5] Meanwhile, non-unidirectional MM are engineered by removing a single methyl allylic to the central alkene, resulting in energetically equivalent opposing photoisomer directions.[16] In some studies, several different classes of slow[11] or fast[16] MM are employed. This strategy is especially powerful to isolate the effects of molecular motion.

As an example, Figure 1 shows a set of MM tested for their ability to stimulate mechanosensitive calcium waves in HEK293 cells.[16] These MM were appended with amine moieties to allow for their activation with visible light and their direct observation with fluorescence microscopy.[9,16] The MM library (Figure 1a) employed two distinct classes of fast MM with different stator structures (MM **1** and MM **2**), one class of slow-rotating controls (MM **3** and MM **5**), and a bidirectional control (MM **4**). One of the slow MM (MM **3**) was found to have a lower absorption coefficient for the wavelength of light being used; therefore, this MM was used at 3× the concentration and stimulated with 2× the light intensity of the other molecules. MM **3** was further supplemented with another slow MM (MM **5**) containing the same rotor and stator but lacking the appended aniline group. The aniline groups served to introduce a bathochromic (red)-shift the absorption spectrum of each molecule to permit

activation with visible light. However, since MM with a fluorene stator, like MM **3** and MM **5**, naturally possess a more red-shifted absorption spectrum than MM with a sulfur-bearing stator, the use of a fluorene-based MM without the appended aniline group resulted in an increased molar absorption coefficient in MM **5** when compared to MM **1**.[16] In addition to the absorption coefficient, the partition coefficient and polar surface area of each MM were taken into consideration to ensure that the MM were as comparable as possible. Comparing the MM for their propensity at stimulating calcium waves revealed that the two fast, unidirectional motors robustly elicited calcium transients, while the slow and bidirectional MM did not (Figure 1b).[16]

This exercise illustrates the strategy behind the selection of MM for a coherent study of photomechanical behavior. We have consistently exercised this methodology across all our research involving the use of MM for biological applications. In aggregate, the results show a consistent hierarchy of effectiveness: fast MM drive more activity than bidirectional MM, which, in turn, drive more activity than slow MM or solvent-only controls (Figure 2).

When the results of our studies do not follow this consistent hierarchy, it is an indication that other light-driven phenomena, including photodynamic or photothermal effects, might be in play. We recently investigated another class of motors[23] based on an hemithioindigo core, for antibacterial applications (Figure 3a). In this specific study, our experiments showed that hemithioindigo switches (HTI **5-7**) displayed a higher bactericidal potency than unidirectionally rotating motors (HTI **1-4**; Figure 3b). Further investigation revealed that the killing of bacteria by these molecules was mitigated by the presence of free radical scavengers (Figure 3c). Therefore, through these and a set of complementary confirming experiments, we concluded that this set of molecules killed bacteria by acting as photosensitizers and generating ROS.

The photodynamic action of the hemithioindigo motors stands in stark contrast to our classic experiments with overcrowded alkene motors, in which slow motors do not kill cells despite generating more ROS than fast-rotating motors.[11] Nonetheless, we were able to

identify a non-photomechanical mechanism of action through the use of slow and non-rotating controls. These two case studies underscore the importance of control systems that closely approximate the properties of rotationally active molecules when working with MM. In hemithioindigo motors, our experiments pointed to photodynamic effects as the mechanism of cell death. In overcrowded alkene motors, the Feringa-type, our experiments pointed to photomechanical effects.

Other concepts for non-rotating control motors can also be found in the literature. In experiments using overcrowded alkene motors, studies often employ the isolated "stator" or "rotor" halves of the full motor as a non-rotating control (Figure 4a).[24] These molecules are attractive as controls since they are intrinsically chemically analogous to the active motor compound. However, they can have drastically different optical properties due to a difference in the size of the conjugated system. Therefore, researchers should account for this by including optical characterization when employing these controls. Furthermore, episulfide-locked variants of overcrowded alkene-based motors have also been used as controls in various biological[15] and materials studies (Figure 4b).[25] These molecules are excellent controls since they closely approximate the structure of the active motor while also possessing a similar molecular weight. With the episulfide, however, desulfurization can occur, resulting in the photoactivated crowded alkene motor. Hence, further tests must be done to ensure the episulfide integrity. Both the isolated rotor and stator and the locked variants, employed strategically, can be useful as negative controls intended to isolate the effects of molecular motion in biological experiments.

Further mechanistic experiments can be employed to investigate the hypothesis of a mechanical mode of action. Gadolinium ions (Gd^{3+}) administered to cells can modulate the fluidity and electrostatic potential of the phospholipid bilayer.[26,27] This effect can be used pharmacologically to determine whether the membrane properties have any bearing on the mechanism of elicited biological action. Similarly, the disruption of either actin filaments (by

Cytochalasin D) or microtubules (by nocodazole) can be used as mechanistic experiments to determine the effects of mechanical force transmission across the cytoskeleton.[28] The cytoskeleton maintains cellular structural integrity and is known to play a role in the transmission of mechanical force and mechanosensitive signaling pathways.[29]

We previously used both Gd^{3+} and Cytochalasin D to investigate the mechanism by which MM elicited intracellular calcium signals. Gd^{3+} had no effect, indicating that extracellular mechanical forces or mechanosensitive plasma membrane channels likely did not contribute to MM-induced cellular calcium transients. However, disruption of the cytoskeleton by Cytochalasin D completely abolished these calcium transients,[16] indicating that MM might drive intracellular signaling by affecting the cytoskeleton.[14] This is consistent with fluorescence microscopy results which showed that in HEK293 cells, most of the MM conjugated with anilines were internalized within cells and not embedded within the plasma membrane.

3. Investigating the Effects of ROS.

The generation of ROS should be considered when irradiating any light-absorbing fluorophore with light, even a MM. Various experimental strategy can be employed to identify potential contributions of ROS in photostimulation experiments. Our previous work has tracked the production of ROS in mammalian cells using ROS-sensitive fluorescent dyes, such as MitoROS, and comparing the production of ROS by MM to that elicited by a photosensitizer (chlorin e6) or MM in the presence of a free radical scavenger, *N*-acetyl cysteine (NAC).[9] We have found that the most useful experiments for isolating the effects of ROS are those employing of ROS scavengers, such as NAC, at high concentrations (~1 mM or higher) under the photoactivation conditions.[11,23,30] These experiments effectively differentiate ROS-driven processes (Figure 3) from processes driven by molecular mechanical action, and they remain applicable for both lipophilic and hydrophilic motor designs.[31,32]

We provide an example of the use of ROS scavengers in MM experiments in Figure 5, where we conduct a series of time-to-necrosis experiments using a mouse fibroblast cell line (NIH 3T3) and fast-rotating MM **6** (Figure 5a) at varying concentrations. When this MM is activated with 355 nm light, propidium iodide (PI) is eventually detected within the nucleus of the cell. The time-to-necrosis is defined as the first time point at which a detectable amount of PI uptake into the nucleus occurs and serves to differentiate the rate of membrane permeabilization between different conditions. We determined the time-to-necrosis in the presence and absence of MM **6** and various ROS scavengers. Figures S2-S8 show the raw micrographs used to generate this data.

We employed the superoxide and hydroxide radical scavenger NAC[33,34] and the superoxide scavenger thiourea (TU),[35] which are well-tolerated by and effective in most cell types, including NIH 3T3 cells. Irradiation of cells treated with 0.5 μM of MM causes rapid cell death (Figure 5b-c), with a time-to-necrosis of ~290 s, regardless of the concentration of NAC or TU (Figure 5d). Interestingly, the addition of NAC has a small impact on the time taken for UV-induced necrosis to occur in the absence of MM **6**. In the absence of NAC, PI uptake is first observable 510 s after irradiation of the control slide. In the presence of 1 mM NAC, PI uptake is first observable after 690 s (Figure 5d). This result is consistent with the idea that the UV light (355 nm) eventually causes necrosis of cells by a photodynamic mechanism.[36]

We then test the effects of MM at 100x higher concentrations. These experiments give more ambiguous results. At a 50 μM concentration of MM **6**, the time-to-necrosis is similar (~290 s) and remains constant at 0 mM, 1 mM, and 5 mM of NAC (Figure 5e). However, the time-to-necrosis increases by ~90 s in the presence of higher (1 mM to 5 mM) concentrations of TU (Figure 5f). This is not observed at low (0.5 μM) concentrations of MM **6**. These results underscore the fact that different processes may take effect in different concentration regimes. This observation is in agreement with the literature, which shows that the photoisomerization yield of MM can decrease at higher concentrations due to aggregation in a phenomenon known

as aggregation-induced emission.[37] Judging by the results obtained with TU, at large concentrations (~50 μM) of this MM, a photodynamic effect can contribute to MM-induced cell death. However, at lower concentrations (~0.5 μM), the data do not support the presence of a photodynamic contributor. These excessive concentration effects can lead to erroneous results, suggesting a photodynamic mechanism of action while masking a mechanical effect. Such misleading data is further exacerbated when no slow-rotating or other control molecules are used.[22] While the cellular trafficking and localization of MM is expected to remain similar across different concentration regimes (Figure S9 and Table S1), even in the event that a larger portion of MM become localized to the cell membrane or intracellular compartments, this change would not be expected to affect the sensitivity of MM activation to typical ROS scavengers.[38]

These experiments with free radical scavengers remain important even in the cases where fast MM elicit the desired biological effect and slow MM do not. Singlet oxygen generation is often possible when irradiating a fluorophore with energetic light. Therefore, we may eventually encounter a class of MM that works through a synergy of photosensitization and molecular motion. For example, in *Candida albicans,* MM cause a series of biological changes related to mitochondrial dysfunction (Figure 6).[12] Although *C. albicans* were insensitive to slow-rotating MM, fluorescence microscopy experiments with MM **1**-treated *C. albicans* revealed the production of ROS during irradiation (Figure 6a-b). It is unclear whether this increase in ROS concentration is due to the photodynamic action of MM or photomechanically induced disruption of cellular respiration. However, even though the ROS levels of cells return to normal after stimulation, the cells eventually necrose. Furthermore, treatment of *C. albicans* with the mitochondria-specific ROS scavenger MitoTempo is insufficient to prevent necrosis despite keeping ROS levels at pre-stimulation conditions (Figure 6c-d). This indicates that ROS produced during irradiation is not directly driving the necrotic death of *C. albicans.*

Finally, when using controls with different rotary properties, a direct investigation of the capability of each molecule to generate ROS can also be helpful. Figure 7 shows additional experiments conducted with the free radical detector 1,3-diphenylisobenzofuran (DPBF) using the previously presented fast and slow-rotating MM **1** and MM **3**, respectively. In addition to the fast MM and the slow MM, we also test for DPBF decomposition in the absence of any photosensitizer. DPBF is a highly sensitive ROS detector and may decompose even when exposed to the small amount of ROS generated by simple photolysis in the absence of a photosensitizer (Figure 7a).[39] Despite this sensitivity, the addition of 8 μM of fast-rotating MM **1** or slow-rotating MM **3** does not result in additional DPBF decomposition under the same irradiation conditions (Figure 7b-d). We also confirm that the photodecomposition of DPBF is attributable to ROS generation by conducting a control experiment using sodium azide (40 mM) as a quencher (Figure 7d). The inclusion of sodium azide results in much less decomposition ($P = 0.008 < 0.01$) than under typical conditions.

4. Investigating the Effects of Heating.

Local heat generation can also influence the responses of cells to photostimulation. Previous experiments have shown that an increase in temperature to 42 °C can potentiate the sensitivity of tumors to conventional treatments by affecting blood flow, nutrient supply, and immune responsiveness, while an increase in temperature to 45 °C results in death by necrosis.[40] Thermal stimulation can also lead to intracellular calcium release,[41] enhanced diffusion,[42] and other phenomena that might be confused with photomechanical effects driven by MM.

In a photothermal process, heat is generated by the irradiation of a system containing a light-absorbing thermal agent, commonly a molecular dye or nanoparticle. In this system, incident photons are absorbed by the thermal agent, which then transfers this energy to the surrounding tissue. Therefore, the relative amount of heat generated in this process is related to

the amount of light absorbed by the thermal agent, which is described by the Beer-Lambert Law:[43]

$$I = I_0 e^{-\varepsilon l c}$$

Equation 1: The Beer-Lambert Law.

Where ε describes the molar absorption coefficient, l describes the path length, c describes the concentration, I_0 describes the initial light intensity, and I describes the light intensity after absorption. Therefore, the amount of heat generated in a photothermal process is tied to the concentration and absorption coefficient of the thermal agent.

Our previous work has measured temperature elevation in the culture medium during photostimulation experiments and compared them across control groups, showing that cells do not experience additional heat in the presence of fast MM.[9,11] Meanwhile, *in vivo,* the temperature of irradiated tumors can be directly monitored.[44,45] However, the measurement of the suspension or tissue temperature may not account for localized heating at the cellular level. Therefore, experiments with slow MM with a similar or higher molar absorption coefficient play an important role in revealing potential photothermal effects in our experiments.[9,11]

In some systems, molecular motion itself has been suggested to cause temperature spikes that can be used for medical purposes such as photothermal therapy. In particular, studies have shown that the molecular motion of triazide[46] and triphenylamine[47] moieties and tetraphenyethylene motors[17] can contribute to increases in temperature that can be used for effective photothermal therapy. This phenomenon was termed “intramolecular motion induced photothermy”, or iMIPT.[17] Similar to the examples covered thus far, these experiments use controls with different rotary properties. For example, Zhang *et al.* investigated tetraphenylethylene (TPE) motors by controlling their aggregation characteristics using spacers of variable length (Figure 8).[17] The quantum yield of photoisomerization in these systems

decreases upon aggregation. Therefore, by attaching alkyl spacers to actuating molecules, aggregation can be prevented, resulting in higher levels of molecular motion that are then linked to elevated temperature.

In future experiments, the amount of local heating at the cellular level can be tracked by fluorescent methods. The quantum yield of fluorescence in a fluorophore is temperature-dependent, allowing changes in local fluorescence to be used as an approximate indicator of local temperature. Yoo *et al.* previously used the fluorescence of transfected mCherry, a red fluorescent protein, to assess local heating in primary cortical neurons treated with ultrasound.[48] Marino *et al.* took this methodology a step further and used a "fluorescent thermometer," a molecule whose fluorescence was especially sensitive to local temperature changes, to assess local heating in C2C12 myotubes.[49] Accordingly, fluorescence can be a valuable tool in assessing local temperature changes that may drive processes like cell death. Finally, changes in the expression of heat shock proteins can be employed to assess potential photothermal effects.[19]

5. Conclusion.

MM hold great promise for biological materials applications leveraging their unique photomechanical properties. However, to expand our understanding of MM-based biotechnology, it is essential that the effects they elicit are correctly attributed to photomechanical, photothermal, or photodynamic driving forces. Our intent in delivering this perspective is to share the methodology we use for the identification of effects that depend on rapid, unidirectional molecular rotation that mechanically disrupt biological materials.

These criteria critically involve comparison of control motors of similar optical and physicochemical properties. The inclusion of a slow or non-rotating motor is essential for the identification of effects that depend on molecular rotation. Ideally, optical characterization should also be included to provide information regarding possible photothermal effects.

Furthermore, experiments with ROS scavengers and detectors as well as direct measurement of suspension temperature can offer additional information about the propensity of the molecules employed to generate ROS or cause temperature elevations. These and other experiments presented in this article have thus far been effective at isolating the mechanical effects of molecular motion in biological materials,[8] identifying effects that are driven exclusively by non-motion driven effects,[23] and even identifying potential synergies between the different effects.[12] We hope that this framework spurs the development of new and interesting techniques using MM.

Conflict of Interest

Rice University owns intellectual property on the use of electromagnetic (light) activation of MM for the killing and treating of cells. This intellectual property has been licensed in part to a company in which J.M.T. is a stockholder, although he is not an employee, officer, or director of that company. Conflicts of interest are mitigated through regular disclosure to the Rice University Office of Sponsored Projects and Research Compliance. The authors declare no other potential conflicts.

Data Availability Statement

The data supporting the findings of this study are contained within the article.

Supporting Information

Supporting Information is available from the Wiley Online Library or from the author.

Acknowledgements.

J. L. B. and T. S. B. contributed equally to this work. This project received funding from the European Union's Horizon 2020 research and innovation programme under the Marie Skłodowska-Curie grant agreement No. 843116 (A.L.S), National Science Foundation Graduate Research Fellowship Program (J.L.B.), The Discovery Institute (J.M.T.), and the Robert A. Welch Foundation (C-2017-20220330) (J.M.T.). V.G.-L. holds a Career Award at the Scientific Interface from the Burroughs Welcome Fund. R.P. and T.S.B. acknowledge support from the Royal Society University Research Fellowship URF\R\191002, BBSRC BB/S017615/1, BB/X001172/1 and EPSRC EP/X040259/1. The funders had no role in the study design, data collection and analysis, decision to publish, or preparation of the manuscript.

Received: ((will be filled in by the editorial staff))

Revised: ((will be filled in by the editorial staff))

Published online: ((will be filled in by the editorial staff))

References

[1] N. Koumura, R. W. J. Zijlstra, R. A. van Delden, N. Harada, B. L. Feringa. *Nature* **1999**, *401*, 152.

[2] D. Roke, S. J. Wezenberg, B. L. Feringa.. *Proc. Nat. Acad. Sci.,* **2018**, *115*, 9423.

[3] V. García-López, D. Liu, J. M. Tour. *Chem. Rev.* **2020,** *120*, 79.

[4] M. M. Pollard, M. Klok, D. Pijper, B. L. Feringa. *Adv. Func. Mater.* **2007**, *17*, 718.

[5] M. Klok, N. Boyle, M. T. Pryce, A. Meetsma, W. R. Browne, B. L. Feringa. *J. Am. Chem. Soc.* **2008**, *130*, 10484.

[6] A. Saywell, A. Bakker, J. Mielke, T. Kumagai, M. Wolf, V. García-López, P.-T. Chiang, J. M. Tour, L. Grill. *ACS Nano* **2016**, *10*, 10945.

[7] V. García-López, P.-T. Chiang, F. Chen, G. Ruan, A. A. Martí, A. B. Kolomeisky, G. Wang, J. M. Tour. *Nano Lett.* **2015,** *15*, 8229.

[8] V. García-López, F. Chen, L. G. Nilewski, G. Duret, A. Aliyan, A. B. Kolomeisky, J. T. Robinson, G. Wang, R. Pal, J. M. Tour. *Nature* **2017**, *548*, 567.

[9] C. Ayala-Orozco, D. Liu, Y. Li, L. B. Alemany, R. Pal, S. Krishnan, J. M. Tour. *ACS Appl. Mater. Int.* **2020***, 12*, 410.

[10] T. Galbadage, D. Liu, L. B. Alemany, R. Pal, J. M. Tour, R. S. Gunasekera, J. D. Cirillo. *ACS Nano* **2019**, *13*, 14377.

[11] A. L. Santos, D. Liu, A. K. Reed, A. M. Wyderka, A. van Venrooy, J. T. li, V. D. Li, M. Misiura, O. Samoylova, J. L. Beckham, C. Ayala-Orozco, A. B. Kolomeisky, L. B. Alemany, A. Oliver, G. P. Tegos, J. M. Tour. *Sci. Adv.,* **2022**, *8*, eabm2055.

[12] A. L. Santos, J. L. Beckham, D. Liu, G. Li, A. van Venrooy, A. Oliver, G. P. Tegos, J. M. Tour. *Adv. Sci.* **2023,** *10*, 2205781.

[13] K. Liu, J. Sun, C. Ma, S. Maity, F. Wang, Y. Zhou, G. Portale, R. Gostl, W. H. Roos, H. Zhang, A. Hermann. *Angew. Chem.* **2021,** *60*, 3222.

[14] W.-Z. Wang, L.-B. Huang, S.-P. Zheng, E. Moulin, O. Gavat, M. Barboiu, N. Giuseppone. *J. Am. Chem. Soc.* **2021**, *143*, 15653.

[15] Y. Zheng, M. K. L. Han, R. Zhaoe, J. Blass, D. W. Zhou, J.-R. Colard-Itté, D. Dattler, A. Colak, M. Hoth, J. A. García, B. Qu, R. Bennewitz, N. Giuseppone, A. del Campo. *Nat. Commun.* **2021**, *12*, 3580.

[16] J. L. Beckham, A. R. van Venrooy, S. Kim, G. Li, B. Li, G. Duret, D. Arnold, X. Zhao, J. T. Li, A. L. Santos, G. Chaudhry, D. Liu, J. T. Robinson, J. M. Tour, J. M. *Nat. Nanotechnol.* **2023,** https://doi.org/10.1038/s41565-023-01436-w.

[17] L. Ribovski, Q. Zhou, J. Chen, B. L. Feringa, P. S. van Rijn, I. Zuhorn. *Chem. Commun,* **2020**, *56*, 8774.

[18] Z. Zhao, C. Chen, W. Wu, F. Wang, L. Du, X. Zhang, Y. Xiong, X. He, Y. Cai, R. T. K. Kwok, J. W. Y. Lam, X. Gao, P. Sun, D. L. Phillips, D. Ding, B. Z. Tang. *Nat. Commun.,* **2019**, *10*, 768.

[19] B. Guo, Z. Huang, Q. Shi, E. Middha, S. Xu, L. Li, M. Wu, J. Jiang, Q. Hu, Z. Fu, B. Liu. *Adv. Func. Mater.* **2020**, *30*, 1907093.

[20] D. Zhi, T. Yang, J. O'Hagan, S. Zhang, R. F. Donnelly. *J. Contr. Rel.,* **2020**, *325*, 52.

[21] S. S. Lucky, K. C. Soo, Y. Zhang. *Chem. Rev.* **2015**, *115*, 1990.

[22] A. M. Firsov, J. Pfeffermann, A. S. Benditkis, T. I. Rokitskaya, A. S. Kozlov, E. A. Kotova, A. A. Krasnovsky, P. Pohl, Y. N. Antonenko. *J. Photochem. Photobiol. B.: Biol.* **2023**, *239*, 112633.

[23] A. L. Santos, A. van Venrooy, A. K. Reed, A. M. Wyderka, V. Garcia-Lopez, L. B. Alemany, A. Oliver, G. P. Tegos, J. M. Tour. *Adv. Sci.,* **2022,** *9*, 2203242.

[24] Q. Zhou, J. Chen, Y. Luan, P. A. Vainikka, S. Thallmair, S. J. Marrink, B. L. Feringa, P. van Rijn. *Sci. Adv.* **2020,** *6*, aay2756.

[25] Q. Li, G. Fuks, E. Moulin, M. Maaloum, M. Rawiso, I. Kulic, J. T. Foy, N. Giuseppone. *Nat. Nanotechnol.* **2015**, *10*, 161.

[26] F. Guilak, R. A. Zell, G. R. Erickson, D. A. Grande, C. T. Rubin, K. J. McLeod, H. J. Donahue. *J. Orthop. Res.* **1999**, *17*, 421.

[27] Y. A. Ermakov, A. Z. Averbakh, A. I. Yusipovich, S. Sukharev. *Biophys. J.* **2001**, *80*, 1851.

[28] C. M. P. Ribeiro, J. Reece, J. W. Putney. *J. Biol. Chem.,* **1997**, *272*, 26555.

[29] T.-J. Kim, C. Joo, J. Seong, R. Vafabakhsh, E. L. Botvinick, M. W. Berns, A. E. Palmer, N. Wang, T. Ha, E. Jakobsson, J. Sun, Y. Wang. *eLife* **2015**, *4*, e04876.

[30] C. Ayala-Orozco, D. Galvez-Aranda, A. Corona, J. M. Seminario, R. Rangel, J. N. Myers, J. M. Tour, *bioRxiv*, preprint, DOI: 10.1101/2023.01.25.525400.

[31] H. Kim, J. Lee, C. Oh, J.-H. Park. *Nat Commun* **2017**, *8*, 15880.

[32] Y. Bu, T. Xu, X. Zhu, J. Zhang, L. Wang, Z. Yu, J. Yu, A. Wang, Y. Tian, H. Zhou, Y. Xie. *Chem. Sci.* **2020**, *11*, 10279.

[33] Y. Samuni, S. Goldstein, O. M. Dean, M. Berk. *Biochim. Biophys. Acta,* **2013**, *1830*, 4117.

[34] M. P. Murphy, A. Holmgren, N.-G. Larsson, B. Halliwell, C. J. Chang, B. Kalyanaraman, S. G. Rhee, P. J. Thornalley, L. Partridge, D. Gems, T. Nyström, V. Belousov, P. T. Schumacker, C. C. Winterbourn. *Cell Metab.* **2011**, *13*, 361.

[35] H. Takahashi, A. Nishina, R.-H. Fukumoto, H. Kimura, M. Kotetsu, H. Ishihara. *Life Sci.,* **2005,** *76*, 2185.

[36] T. L. de Jager, A. E. Cockrell, S. S. Du Plessis. Ultraviolet Light Induced Generation of Reactive Oxygen Species. In *Ultraviolet Light in Human Health, Diseases and Environment; Advances in Experimental Medicine and Biology.* 1st ed; Springer, **2017**, 996, 15-23.

[37] Y. Ren, J. W. Y. Lam, Y. Dong, B. Z. Tang, K. S. Wong. *J. Phys. Chem. B,* **2005**, *109*, 1135.

[38] H. Kim, J. Lee, C. Oh, J.-H. Park. *Nat. Commun.,* **2017**, *8*, 15880.

[39] T. Entradas, S. Waldron, M. Volk. *J. Photochem. Photobiol. B.: Biol.* **2020**, *204*, 111787.

[40] B. Hildebrandt, P. Wust, O. Ahlers, A. Dieing, G. Sreenivasa, T. Kerner, R. Felix, H. Riess. *Crit. Rev. Oncol.* **2002**, *43*, 33.

[41] D. Zhu, L. Feng, N. Feliu, A. H. Guse, W. J. Parak. *Adv. Mater.* **2021**, *33*, 2008261.

[42] S. Y. Nishimura, S. J. Lord, L. O. Klein, K. A. Willets, M. He, Z. Lu, R. J. Twieg, W. E. Moerner. *J Phys Chem B* **2006**, *110*, 8151.

[43] G. T. Spence, G. V. Hartland, B. D. Smith. *Chem. Sci.* **2013,** *4,* 4240.

[44] F. Zhou, S. Wu, B. Wu, W. R. Chen, D. Xing. *Small* **2011**, *7*, 2727.

[45] P. Zhao, Z. Jin, Q. Chen, T. Yang, D. Chen, J. Meng, X. Lu, Z. Gu, Q. He. *Nat. Commun.* **2018**, *9*, 4241.

[46] X. W. Liu, W. Zhao, Y. Wu, Z. Meng, Z. He, X. Qi, Y. Ren, Z.-Q. Yu, B. Z. Tang. *Nat. Commun.* **2022**, *13*, 3887.

[47] S. Liu, X. Zhou, H. Zhang, H. Ou, J. W. Y. Lam, Y. Liu, L. Shi, D. Ding, B. Z. Tang. *J. Am. Chem. Soc.* **2019,** *141,* 5359.

[48] S. Yoo, D. R. Mittelstein, R. C. Hurt, J. Lacroix, M. G. Shapiro. *Nat. Commun.* **2022**, *13*, 493.

[49] A. Marino, S. Arai, Y. Hou, A. Degl'Innocenti, V. Cappello, B. Mazzolai, Y.-T. Chang, V. Mattoli, M. Suzuki, G. Ciofani. *ACS Nano,* **2017**, *11*, 2494.

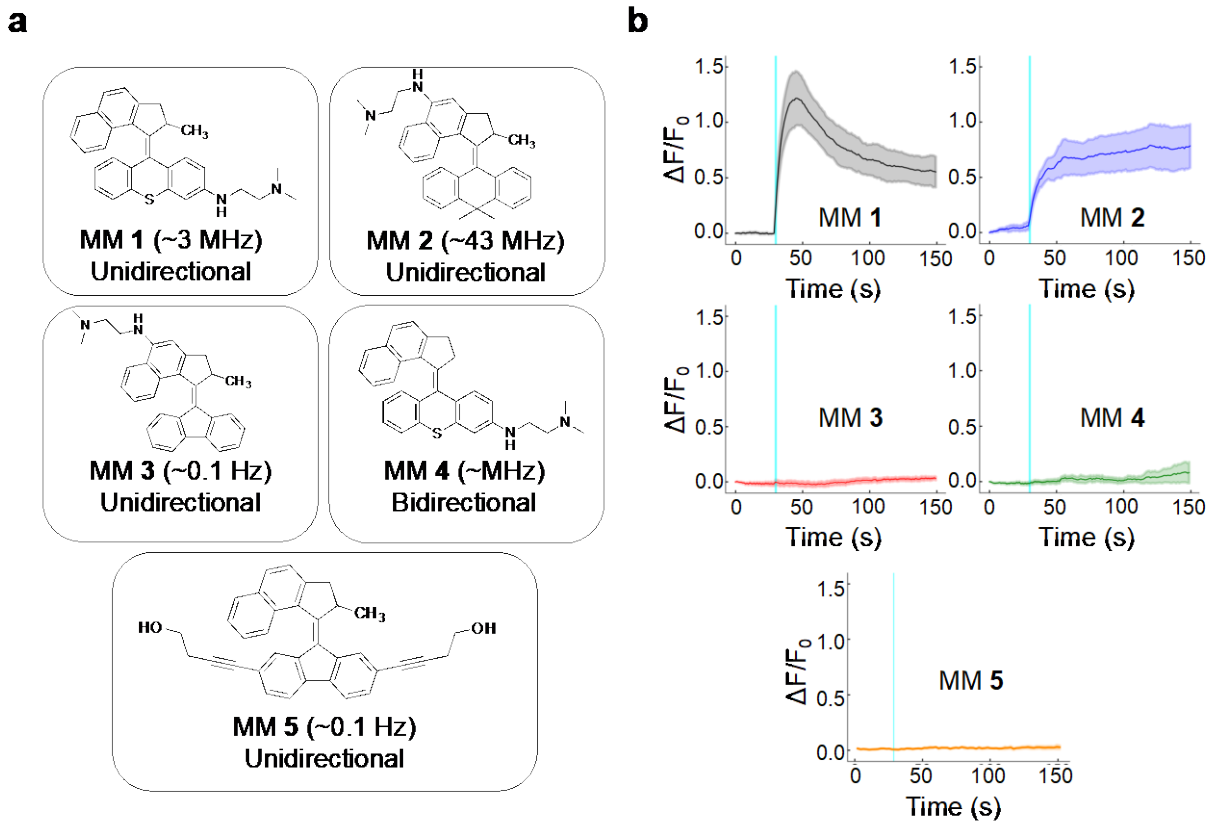

Figure 1. A sample MM test set using multiple classes of fast MM and slow or non-unidirectional control motors[16]. **(a)** The MM set containing fast, unidirectional rotating MM **1** and MM **2**, slow-rotating MM **3** and MM **5**, and bidirectional MM **4**. Blue: Fast, unidirectional MM. Red: Slow or non-unidirectional MM. **(b)** Representative normalized fluorescence intensity traces of calcium-sensitive dye Fluo-4 in HEK293 cells treated with each MM. The solid line represents the average responses of $n \geq 6$ independent cells, and the shaded area represents the standard error of the mean. Images were collected at 0.94 frames per second. Traces were normalized to the first 10 data points. MM **1**, MM **2**, MM **4**, and MM **5** were administered to cells at 8 μM. MM **3** was administered to cells at 24 μM. Stimuli for cells treated with MM **1**, MM **2**, MM **4**, and MM **5** used a 250 ms pulse width delivered to a circular area of diameter 5 μm at 3.2×10^2 W cm^{-2}. Stimuli for cells treated with MM **3** were administered at 6.4×10^2 W cm^{-2}. Irradiation used a 400 nm, 15 mW photodiode laser operating at a pixel dwell time of 140 ms using a 212 μm x 212 μm field of view. For all plots, the cyan line indicates the time of stimulus presentation. Figures adapted from Beckham, J. L. *et al.*[16]

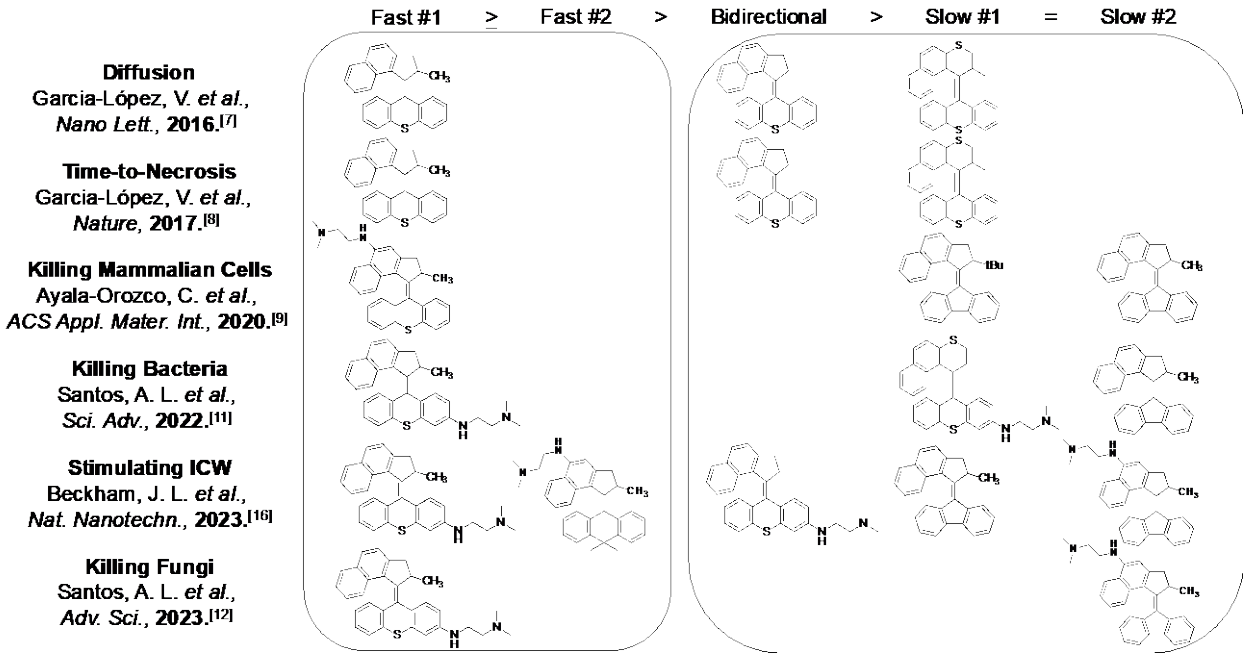

Figure 2. Change in photomechanical potency with respect to MM structure. Examples of MM employed in previous studies by our group with respect to their relative hierarchy of activity. Side chains (other than anilines) were omitted for clarity. Blue: Fast, unidirectional MM. Red: Slow or non-unidirectional MM.

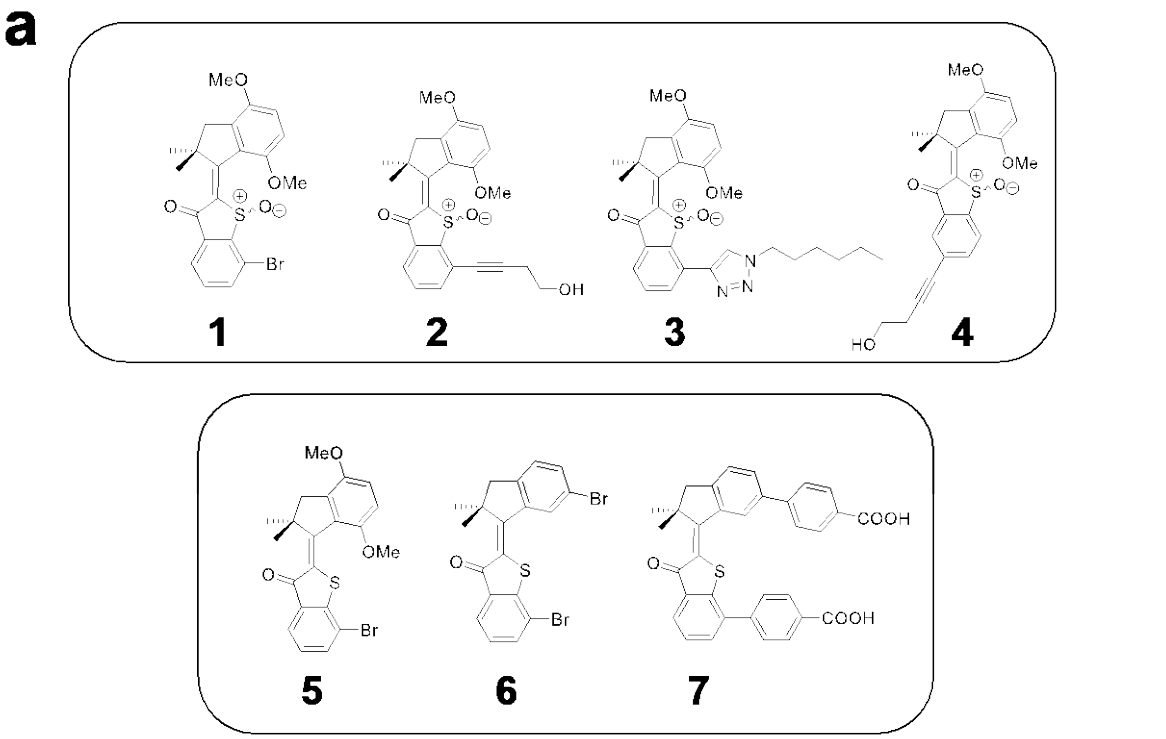
a
MeO
OMe
Br
1
OH
2
N
3
HO
4
COOH
5
6
7
b
B. Megaterium
B. Subtilis
log(N/N0)
Time (min)
HTI 1
HTI 2
HTI 3
HTI 4
HTI 5
HTI 6
HTI 7
1% DMSO
Ciprofloxacin
Gentamicin
c
10-2 10-3 10-4 10-5 10-6
No scavenger, 1% DMSO
No scavenger, 1x MIC HTI 3
DP, 1x MIC HTI 3
NAC, 1x MIC HTI 3
TU, 1x MIC HTI 3

Figure 3. Bactericidal effects and mechanistic experiments of a class of molecules whose biological activity is driven by ROS. **(a)** Structure of hemithioindigo (HTI) molecules **1-7.** Blue: Medium (kHz), unidirectional HTI motors. Red: HTI switches. **(b)** Time-dependent reduction in colony forming units (expressed as the logarithm of base 10 of the ratio between the colony forming unit value at every time point and the colony forming unit value at time zero) of different exponentially growing Gram-positive bacterial strains in the presence of 1% DMSO (solvent control) + 455 nm light at 65 mW cm^{-2}, 1× MIC of each HTI + 455 nm light at 65 mW cm^{-2}, or 2× the MIC of conventional antibiotics. The dashed line denotes the limit of detection of the method. All results are shown as the mean of at least three biological replicates ± standard error of the mean. **(c)** Representative spot plate of *S. aureus* grown with and without iron (DP) or ROS scavengers (NAC, TU) and then challenged with 1% DMSO or 1× MIC of HTI 3 and irradiated with 455 nm light (39 J cm^{-2}). TU: thiourea (1 mM), NAC: *N*-acetyl cysteine (1 mM), DP: dipyridyl (0.5 mM). Figures adapted from Santos, A. L. *et al., Adv. Sci.,* 2022.[23]

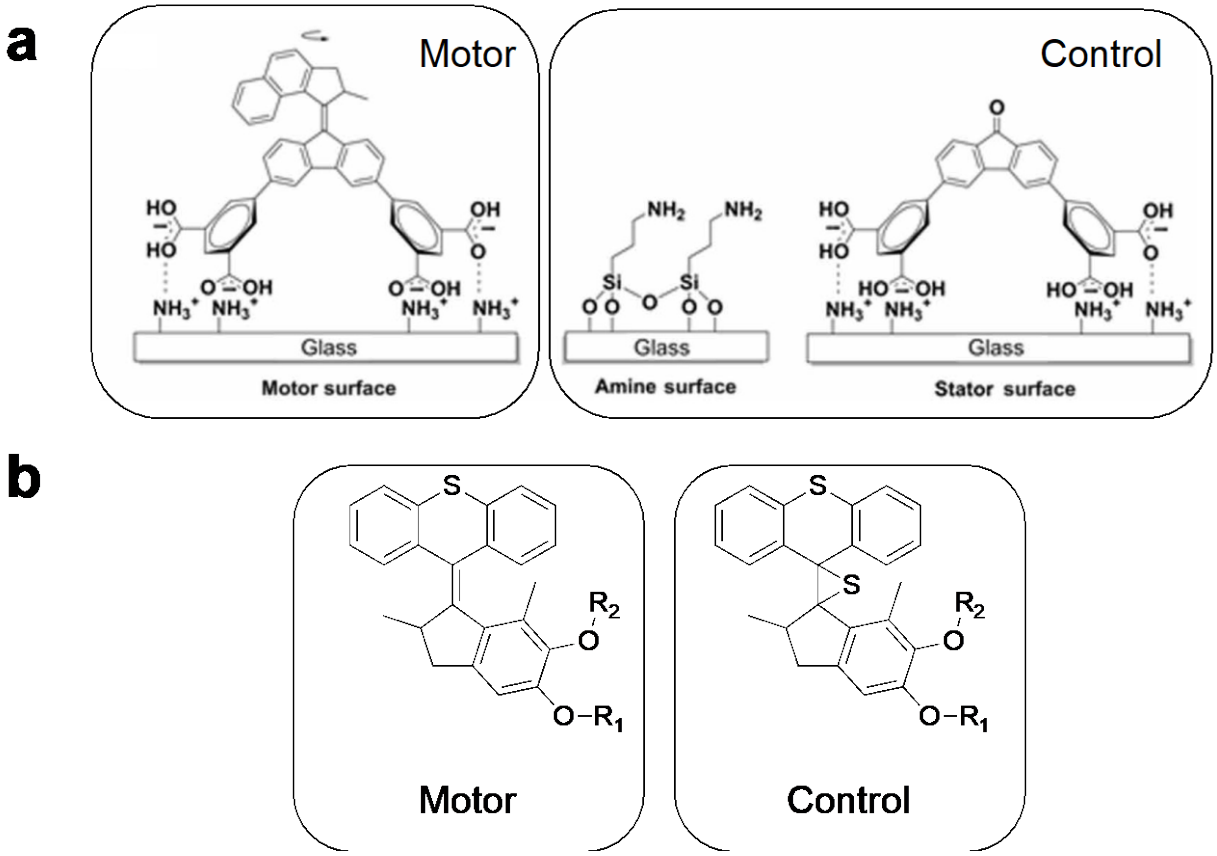

Figure 4. Unidirectionally rotating motors and non-rotating controls from two studies from different groups. **(a)** A unidirectionally rotating, amine, and stator-only control scheme used in Zhou, Q. et al., *Sci. Adv.,* **2020**. Figure adapted with permission[24] **(b)** A fast, unidirectionally rotating motor and a non-rotating episulfide locked control scheme used in Zheng, Y. et al., *Nat. Commun.,* **2021,** *12,* 3580. Figure adapted with permission[15]

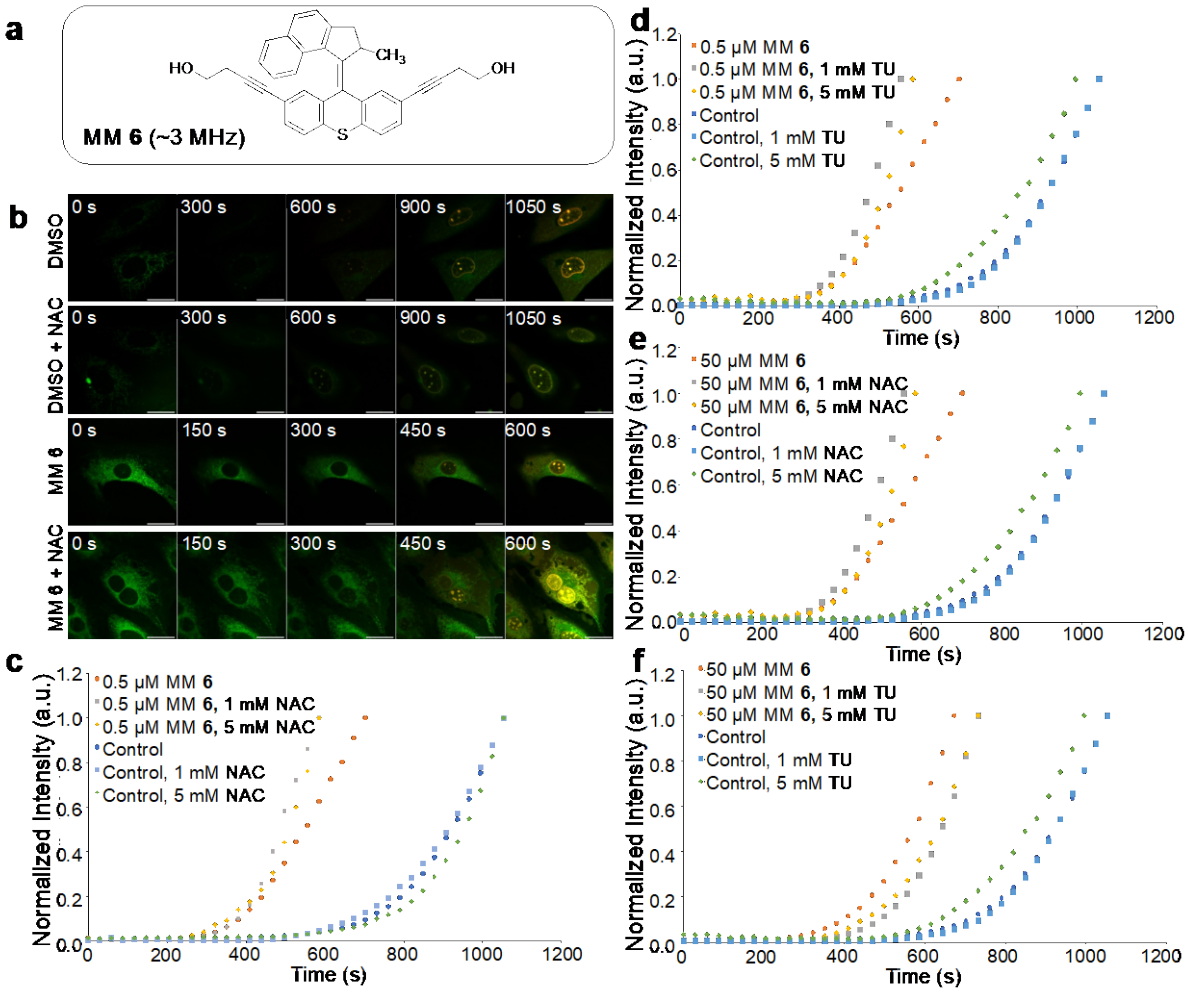

Figure 5. Cell-permeabilizing ability of a fast-rotating MM at various concentrations in the presence of free radical scavengers. **(a)** Structure of MM **6**. **(b)** Microscopic observation of cell death caused by excitation at 355 nm (UV-exposure times are shown for each image), quantified by the observation of PI fluorescence within the nucleus for NIH 3T3 cells loaded with 100 nM PI and either 0.1% DMSO, 0.1% DMSO and 1 mM NAC, 0.5 μM MM **6**, or 0.5 μM MM **6** and 1 mM NAC. All image sets were collected after 30 min incubation after dosing procedure. Overlaid channels of PI fluorescence (λ_{ex} = 543 nm, 0.2 mW; λ_{em} = 600-700 nm), and mitochondrial autofluorescence (λ_{ex} = 355 nm, 20 mW, 400 nJ per voxel; λ_{em} = 440-460 nm). All scale bars are 25 μm. **(c-d)** Normalized fluorescence intensity plots of NIH 3T3 cells treated with different combinations of MM **6** and free radical scavenger **(c)** NAC or **(d)** TU at a low (0.5 μM) concentration of MM **6**. **(e-f)** Normalized fluorescence intensity plots of NIH 3T3 cells treated with different combinations of MM **6** and free radical scavenger **(e)** NAC or **(f)**

TU at a high (50 μM) concentration of MM **6**. Individual data points represent fluorescence values calculated from the mean fluorescence intensity of each image. Images were taken every 30 s.

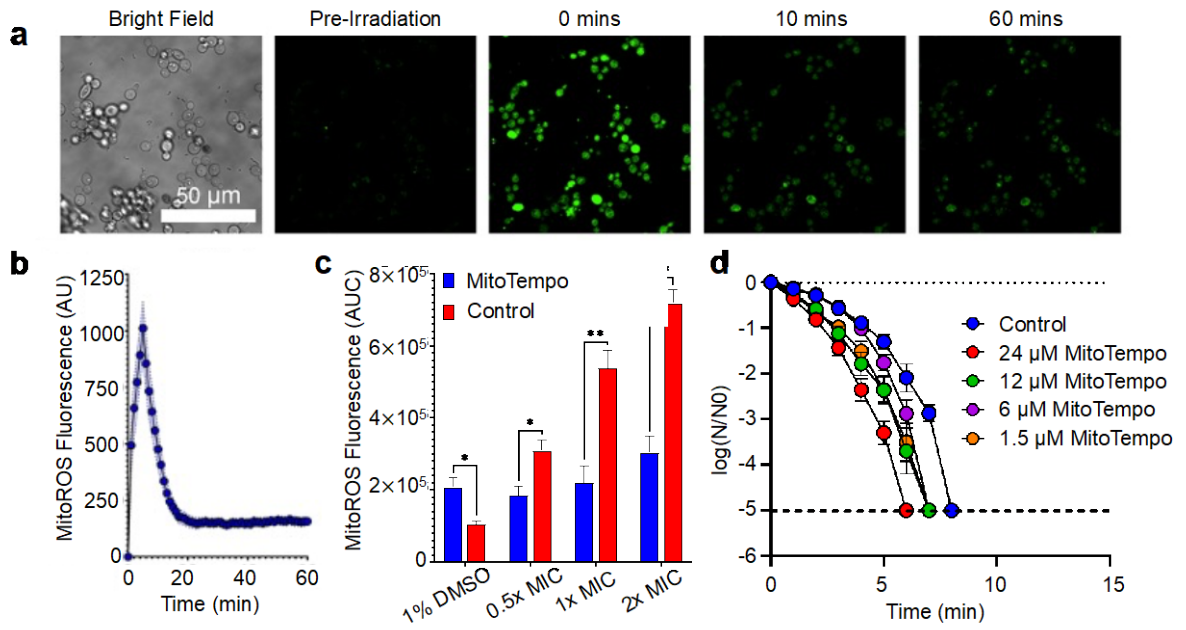

Figure 6. MM cause an increase in mitochondrial ROS in the eukaryotic *C. albicans*, but quenching this ROS is not sufficient to stop cell death. **(a)** Mitochondrial ROS levels detected by confocal microscopy using the MitoROS 580 probe in *C. albicans* treated with MM **1** at 1× the minimum inhibitory concentration (MIC) before and after light activation under the microscope. The bar indicates the scale. **(b)** Temporal profile of MitoROS 580 fluorescence detected by confocal microscopy, shown as the average fluorescence intensity (line) and standard error of the mean (shaded area). **(b)** Fluorescence intensity traces of MitoROS in individual *C. albicans* cells. MM light activation was performed in situ with a SOLA LED using a DAPI excitation filter (395/25 nm, 166 mW cm^{-2} from a 3 W LED) for 5 min. ROS increases during irradiation and decreases after irradiation stops. **(c)** *C. albicans* treated with MM **1** and administered MitoTempo (1.5 µM) experience significantly less ROS production than positive controls. **(d)** Administration of MitoTempo is insufficient to prevent cell death in *C. albicans* treated with MM **1** (1× MIC). Figures adapted from Santos, A. L. *et al.*[12]

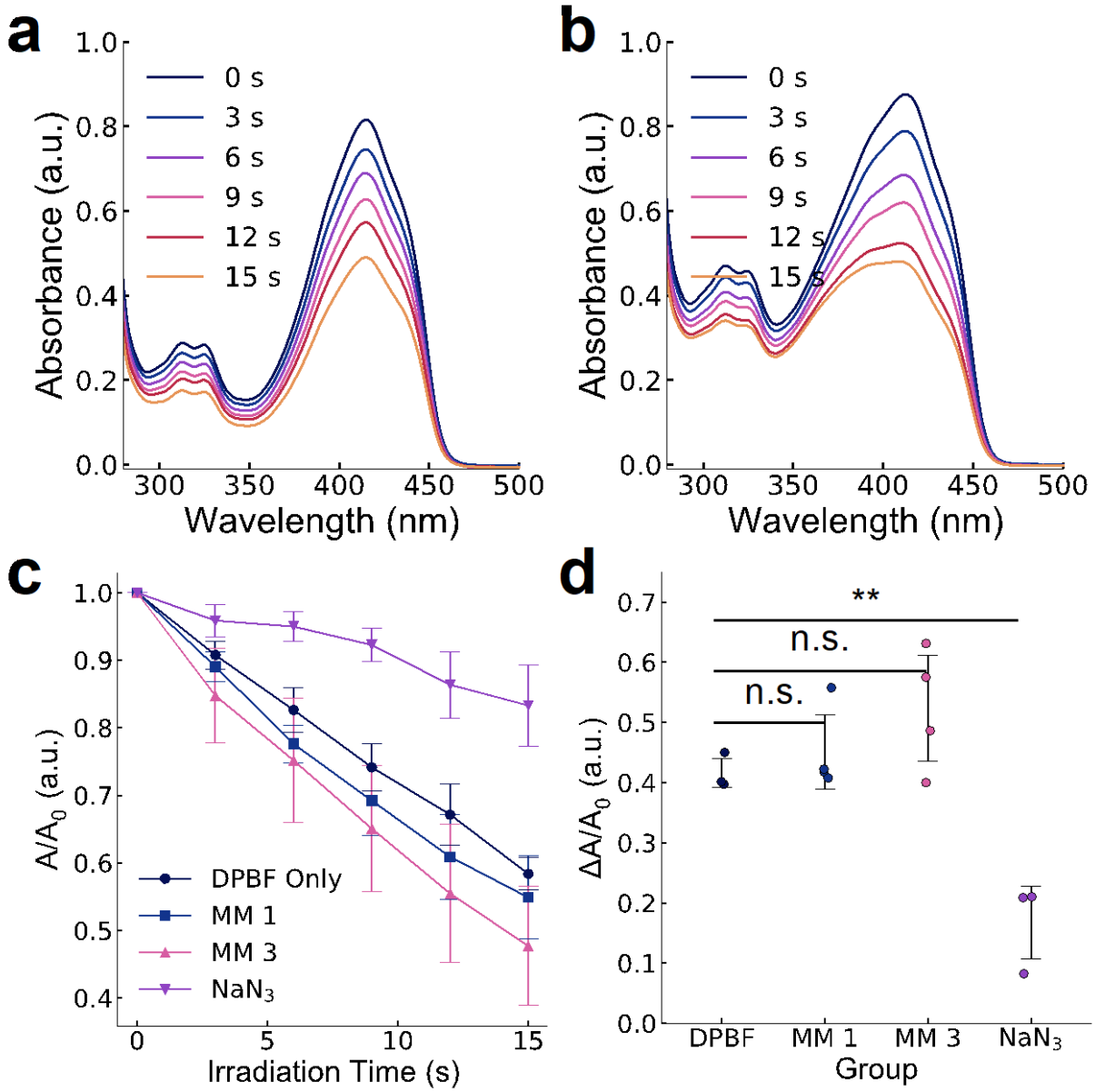

Figure 7. Direct quantification of ROS generation in the presence of various MM using DPBF. **(a)** Absorption spectra of a solution of DPBF (50 µM) in dimethylformamide before and after sequential 3 s doses of 405 nm light. **(b)** Absorption spectra of a solution of DPBF (50 µM) and MM **1** (8 µM) in dimethylformamide before and after sequential 3 s doses of 405 nm light. **(c)** Absorbance at 410 nm over several lengths of irradiation time of solutions containing either DPBF alone (50 µM; n=3), DPBF alongside fast and slow MM (8 µM; n=4), or DPBF in the presence of NaN_3 (40 mM; n=3). Irradiation was conducted using a 405 nm LED (Prizmatix). **(d)** Change in the absorbance of each solution at 410 nm over 15 s of irradiation. Individual

data points are overlaid as a scatter plot. Absorbance is normalized to the starting absorbance. Irradiation was performed using a Prizmatix 405 nm LED at an irradiance of 12.5 mW cm^{-2}. Statistical significance tests were conducted using a one-tailed Welch's t-test. Comparisons marked "n.s." are not significant. ** $P = 0.008051 < 0.01$

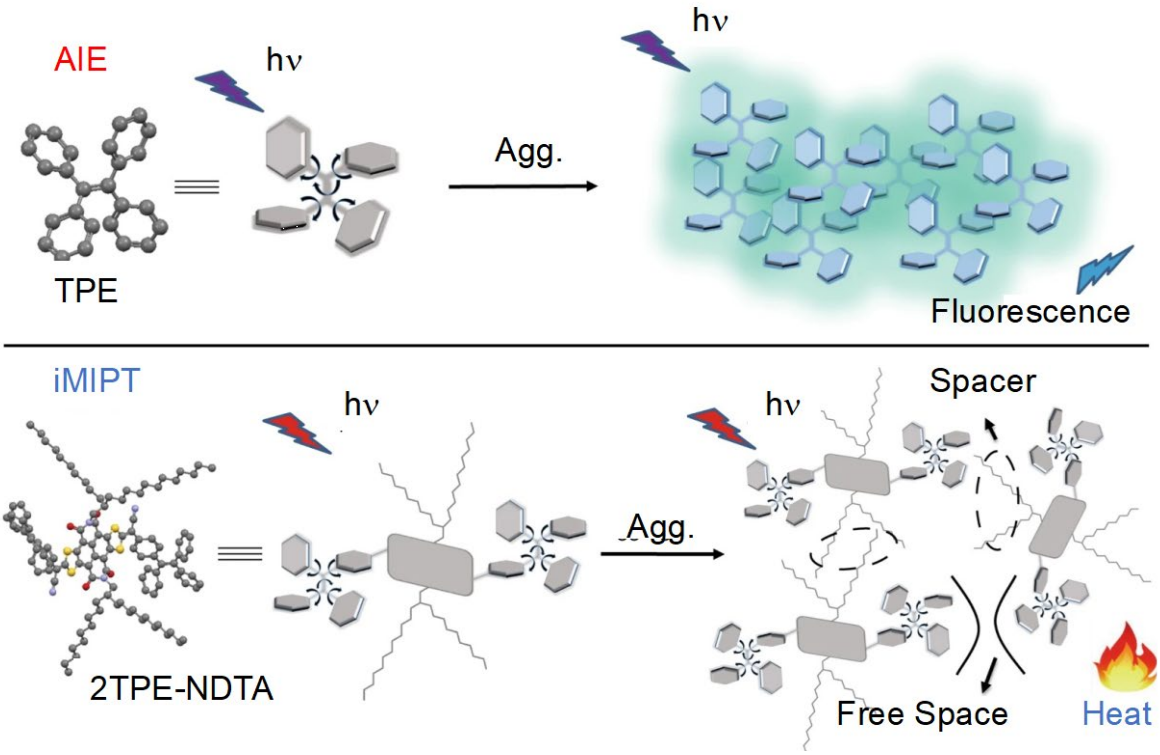

Figure 8. A scheme depicting the design of a photothermal agent based on a tetraphenylethylene (TPE) MM. Top: Unconjugated TPEs aggregate in biological systems, resulting in fluorescent aggregates as the quantum yield of photoisomerization is diminished. Bottom: TPEs attached to naphthalene diimide-fused 2-(1,3-dithiol-2-ylidene)acetonitriles with long alkyl chains, which act as spacers to maintain sufficient distance for isomerization. This additional molecular motion results in increased heat generation. AIE: Aggregation-induced emission. iMIPT: Intramolecular motion induced photothermy. Agg.: Aggregation. Figure adapted with permission from Zhao, Z. *et al., Nat. Commun.,* **2019,** *10,* 768.[17]

Table of Contents

Jacob L. Beckham,[#] Thomas S. Bradford,[#] Ciceron Ayala-Orozco, Ana L. Santos, Dallin Arnold, Alexis R. van Venrooy, Víctor García-López, Robert Pal, and James M. Tour**

Distinguishing Molecular Mechanical Action from Photothermal and Photodynamic Behavior

ToC figure

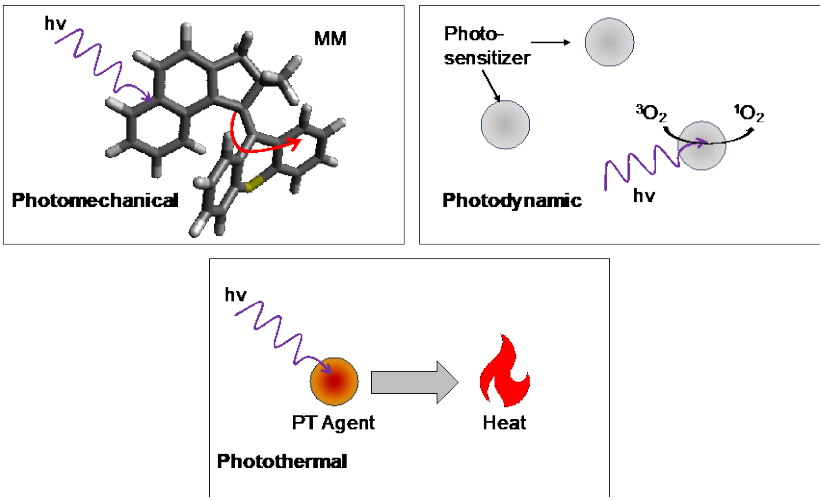

Molecular motors are small molecule actuators that can permeabilize lipid bilayers, kill cancer cells and microorganisms, and control cell signaling. Here, we provide a roadmap detailing how to distinguish the photomechanical action characteristic to these motors from photothermal and photodynamic effects. We hope that this framework leads to a robust criterion for the isolation of the effects of molecular motion as the community seeks to use molecular motors for new and distinctive applications.